NMR Characterization of Substrate Binding in the Phthalate Dioxygenase System†

David L. Tierney,‡,§ George T. Gassner,||,⊥ Claudio Luchinat,*,△ Ivano Bertini,*,▽ David P. Ballou,*,|| and James E. Penner-Hahn*,‡

Departments of Chemistry and Biological Chemistry, University of Michigan, Ann Arbor, Michigan 48109, and Departments of Soil Science and Plant Nutrition and Chemistry, University of Florence, Florence, Italy

Received February 23, 1999; Revised Manuscript Received June 4, 1999

ABSTRACT: The paramagnetic enhancements in the NMR relaxation rates for the fluorine in fluorophthalates have been used to determine the position of the phthalate with respect to the mononuclear metal ion in native and metal-substituted derivatives of phthalate dioxygenase (PDO). These studies show directly that the substrate interacts with the mononuclear metal of PDO and provide the first structural characterization of this interaction. With a molecular mass of 200 kDa, PDO is one of the largest proteins studied to date by paramagnetic NMR. Two paramagnetically broadened ^{19}F lines were observed for monofluorophthalates bound to CoPDO. This demonstrates that fluorophthalate binds to PDO with a handedness, i.e., with the fluorine label facing to the "right" or to the "left", relative to the hyperfine tensor of the Co(II). The relative affinities of the two orientations are slightly different, with a 2-fold and 5-fold excess of the preferred orientation for 4-fluorophthalate and 3-fluorophthalate, respectively. The longitudinal relaxation rate (T_1) and transverse relaxation rate (T_2) data give mutually consistent fluorine to cobalt distances. These results are consistent with approximate bilateral symmetry, with the Co to 3-fluorophthalate distances (∼5.5 Å) approximately 25% longer than the Co to 4-fluorophthalate distances (∼4.5 Å). A detailed geometric model is derived from these data. This structural characterization of the mononuclear site provides a framework to develop hypotheses for the mechanism of oxygenation by the Fe(II)-containing aromatic dioxygenases.

Phthalate dioxygenase (PDO)[1] catalyzes the stereospecific dihydroxylation of phthalate to the 4,5-*cis*-dihydrodiol (Scheme 1). This is the first step in phthalate biodegradation, which uses the catechol cleavage pathway (*1*). Phthalate dioxygenase is a homotetramer of 48 kDa subunits, with each subunit containing a Rieske-type [2Fe-2S] cluster and a mononuclear Fe(II) binding site (*2*). Phthalate dioxygenase reductase (PDR), which contains an FMN and a plant-type [2Fe-2S] center, transfers electrons from NADH to PDO. In the reaction in Scheme 1, NADH donates a hydride to the FMN, and the electrons are passed intramolecularly to the [2Fe-2S] center in PDR; the latter transfers electrons intermolecularly to the Rieske-type [2Fe-2S] cluster of PDO (*3*). The Rieske center then provides electrons sequentially to the mononuclear Fe(II) site, where the hydroxylation reaction is believed to take place.

Scheme 1

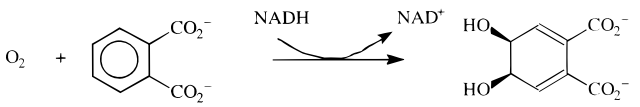

The substrate is bound tightly to the enzyme ($K_d \approx 190$ nM at 4 °C) (*4*). However, in the absence of the mononuclear-site metal, substrate binding is much weaker, with K_d increasing to 2.2 mM. Under steady-state conditions at 4 °C, the apparent k_{cat} for phthalate[2] is 0.8 s^{-1}. In addition to its natural substrate, PDO is capable of binding and hydroxylating a number of substrate analogues that are substituted in either the 3- or 4-positions (*5*). These hydroxylations are nearly as fast as that for the unsubstituted phthalate. For example, 4-F-phthalate turns over with an apparent k_{cat} of 0.4 s^{-1}, only a factor of 2 lower than for phthalate. However, K_d increases by approximately 10-fold for the fluorinated substrates, indicating somewhat weaker binding.

† Supported in part by the NIH (Grant GM-38047 to J.E.P.-H. and GM-20877 to D.P.B.) and by MURST (ex 40%).

* To whom correspondence should be addressed. J.E.P.-H.: phone 734-764-7324; fax 734-647-4865; e-mail jeph@umich.edu. D.P.B.: phone 734-764-9582; fax 734-763-4581; e-mail dballou@umich.edu. C.L.: phone 39-055-4209262; fax 39-055-4209253; e-mail luchinat@cerm.unifi.it. I.B.: phone 39-055-4209272; fax 39-055-4209271; e-mail bertini@cerm.unifi.it.

‡ Department of Chemistry, University of Michigan.

§ Present address: Department of Chemistry, Northwestern University, Evanston, IL 60208-3113.

|| Department of Biological Chemistry, University of Michigan.

⊥ Present address: Department of Chemistry, Massachusetts Institute of Technology, Cambridge, MA 02139.

△ Department of Soil Science and Plant Nutrition, University of Florence.

▽ Department of Chemistry, University of Florence.

[1] Abbreviations: PDO, phthalate dioxygenase from *Burkholderia cepacia;* PDR, phthalate dioxygenase reductase from *B. cepacia*; CoPDO, ZnPDO, and FePDO, phthalate dioxygenase with the mononuclear metal site substituted with Co(II), Zn(II), or Fe(II); apoPDO, phthalate dioxygenase that has been depleted of mononuclear metal; [2Fe-2S], two-iron two-sulfur center; NMRD, nuclear magnetic relaxation dispersion spectroscopy; MCD, magnetic circular dichroism spectroscopy; fwhm, full width at half-maximum.

[2] The apparent k_{cat} values were determined aerobically using 100 μM NADH, 1 μM PDO, 200 nM PDR, and 10 μM ferrous ammonium sulfate in 50 mM HEPES, pH 8 at 25 °C. Although these conditions are not saturating with respect to PDR, they provide reasonable comparisons for the activities with different substrates.

10.1021/bi990431y CCC: $18.00
Published on Web 08/06/1999

Scheme 2

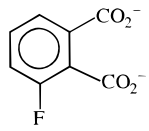

3-fluorophthalate

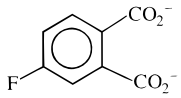

4-fluorophthalate

The PDO mononuclear site has been shown to bind a number of divalent cations (*6*, *7*), although only Fe(II) is able to confer activity. Recent EXAFS (*8*) studies of the mononuclear site are consistent with a six-coordinate metal ion in the resting enzyme. The average first shell bond length decreases ca. 0.05 Å on binding of phthalate, suggesting a decrease in coordination number. Low-temperature MCD studies (*9*, *10*) similarly indicate a decrease in coordination number on binding of substrate. These data clearly demonstrate that phthalate affects the geometry about the mononuclear metal site of PDO and suggest that it does so without directly coordinating to the metal. The MCD data are most consistent with the coordination number changing from six to five on binding substrate. Recent water proton NMRD has identified the displaced ligand as a water molecule (*11*).

To better characterize the interaction of phthalate with the mononuclear metal site of PDO, we have undertaken an NMR study of phthalates labeled with fluorine in either the 3- or 4-positions (Scheme 2) bound to CoPDO, ZnPDO, and FePDO. Crull et al. have previously used ^{19}F NMR to study a fluorine-labeled substrate that is tightly bound to the paramagnetic metalloenzyme cytochrome P-450$_{cam}$ (*12*). In the P-450 studies, it was possible to deduce the spatial relationship of the metal ion with respect to the fluorine on the substrate and to compare this with a crystallographic model of substrate binding. There is no crystal structure available for PDO. However, the structure for a similar enzyme, naphthalene dioxygenase, has recently been solved (*13*) and shows that the mononuclear site is similar to a series of recently determined structures of a variety of oxygenases that contain mononuclear iron (*14*). The accompanying paper (*7*) demonstrates that the mononuclear metal site in PDO is very similar to that of naphthalene dioxygenase, as would be predicted from both its similar function and its sequence similarity (*15*, *16*). Spectroscopic studies (*7*−*11*) have suggested that substrate interacts with the mononuclear metal site of PDO, and the NMR studies presented here now enable us to generate a model for the spatial relationship between the mononuclear metal and the aromatic ring of the phthalate substrate. It can be anticipated that this model will be generally applicable for the binding of substrates to the family of aromatic dioxygenases that contain a Rieske [2Fe-2S] and mononuclear Fe(II) site.

EXPERIMENTAL PROCEDURES

3-Fluorophthalic acid was purchased from Aldrich; 4-fluorophthalate was synthesized by Dr. Bruce Palfey. Phthalate dioxygenase (PDO) was purified from *Burkholderia cepacia*[3] according to published procedures (*2*, *6*). The mononuclear-site metal ion was removed from the purified enzyme (ca. 1 mM) by dialysis against 5 mM EDTA in 50 mM HEPES, pH 7.6, at 4 °C. The dialysis buffer was changed twice over an 18 h period. Residual EDTA was removed by further dialyzing the apoenzyme against 50 mM HEPES at pH 7.6 for 8 h. Metal-substituted derivatives of PDO were prepared by incubating 2 mL of apoenzyme (0.5 mM in subunits) with 1 equiv of Co(II) or Zn(II), added as 15 mM $CoCl_2$ or $Zn(OAc)_2$ in the same buffer. Fe-reconstituted PDO was prepared in a similar fashion, adding an anaerobic solution of 10 mM $Fe(NH_4)_2(SO_4)_2$ to apoenzyme that was preequilibrated with N_2. After approximately 10 min, 2 mL of 50 mM HEPES in D_2O, pH 7.6, containing 0.9 equiv of either 3-F or 4-F-phthalate was added. The resulting solution was concentrated back to 0.5 mL (final concentration of 2 mM in PDO subunits) in a Centricon 30 microconcentrator. Before being loaded into NMR tubes, all samples were degassed and equilibrated with N_2 on a Schlenk line.

The ^{19}F NMR spectra were recorded on a General Electric GN-500Ω NMR spectrometer with a dedicated fluorine probe operating at 470 MHz, without the use of proton decoupling. Sample temperature was maintained (25 °C, unless otherwise noted) with the internal heating coil and thermocouple of the variable temperature unit of the GN-500 and an external Cryocool cooling unit. After the temperature-dependent studies, a room temperature NMR spectrum was acquired at the end of data collection in order to verify the integrity of the samples. For each sample, the temperature-dependent measurements required ca. 2 h at each temperature, for a total experimental time of ca. 10−12 h.

Each spectrum for CoPDO is the average of 50 000−200 000 transients, each consisting of 8K data points, over a spectral window of 200 kHz (acquisition time, A_t = 20.5 ms). For FePDO, A_t was reduced to 13.3 ms (200 000 transients; 4K points; SW = 153 kHz). An 8 μs pulse was used to ensure uniform excitation over the necessary spectral bandwidth. This corresponded to about 40° tilt of the z magnetization. The transmitter was set at the resonant frequency of the free fluorophthalate (−37.2 ppm for 4-F-phthalate; −43.8 ppm for 3-F-phthalate; external trifluoroacetate = 0.0 ppm). Before Fourier transformation, the free induction decay was apodized with an exponential decay, giving 100 Hz line broadening. To optimize data collection for FePDO and CoPDO, a relatively short (80−100 ms) cycle time was used. This time was chosen as being long enough to permit complete relaxation of the paramagnetically affected signals. However, the short cycle times resulted in a significant baseline roll due to probe ringing and incomplete relaxation of the nonparamagnetically relaxed signals. This background was subtracted manually, following the procedure described in detail in Supporting Information.

In all cases, the diamagnetic reference was the corresponding ZnPDO fluorophthalate complex. For ZnPDO, 5000 transients, each consisting of 16K data points, were collected over a 100 kHz bandwidth (A_t = 81.9 ms) with a cycle time of 10 s.

The time constants for longitudinal relaxation, T_1, were measured using a standard inversion−recovery pulse sequence, 180−τ−90−acquire. T_1 experiments for CoPDO and FePDO samples were measured in blocks of 12 500 transients at each τ value, with four blocks being co-added before

[3] The strain has previously been referred to as *Pseudomonas cepacia* DB01 but recently has been classified as belonging to the *Burkholderia* genus [Yabuuchi, E., Kosako, Y., Oyaiso, H., Yano, I., Hotta, H., Hashimoto, Y., Ezaki, T., and Arakawa, M. (1992) *Microbiol. Immunol. 36, 1251*−*1275*].

Fourier transformation. The value of τ was varied nonmonotonically between a minimum of 5 μs and a maximum of 50 ms for paramagnetic samples. A total of 12−15 τ values were used in each determination, requiring approximately 24 h of data collection. For ZnPDO, a total of 7 τ values were used, with a maximum τ of 20 s. The chemical shift differences observed for CoPDO required that each T_1 be determined independently. Apodization of the inversion−recovery data was restricted to 50 Hz line broadening for each τ value, and background subtraction was not performed. T_1 values were determined by nonlinear least-squares fitting of the observed NMR peak amplitudes to an exponential decay.

Data for 4-F-phthalate + CoPDO were also measured on a Bruker MSL-200 spectrometer with the ^{1}H channel tuned to the fluorine frequency of 188 MHz. The final spectrum was obtained by first collecting a background for CoPDO with ^{1}H phthalate to match the dielectric response of the fluorine-containing sample. The spectrum for 4-F-phthalate + CoPDO was then collected under identical conditions. Each FID was the result of averaging 1.5×10^6 transients, each consisting of 1024 data points, over a spectral window of 29.4 kHz (A_t = 17.4 ms), with a cycle time of 20 ms. The FID for the fluorine-free sample was subtracted from the FID for the fluorine-containing sample, and the difference FID was apodized with inclusion of 100 Hz line broadening prior to Fourier transformation.

To verify that the change from phthalate to fluorophthalate did not perturb the Co site, EPR spectra were measured for CoPDO and for CoPDO in the presence of phthalate, 3-F-phthalate, and 4-F-phthalate at 35 GHz in the laboratory of Professor Brian Hoffman (Northwestern University, Evanston, IL) (*17*). EPR signals were detected in dispersion mode under adiabatic rapid passage (*18*); spectrometer conditions are noted in the figure legend.

Paramagnetic Enhancement of Nuclear Relaxation. Paramagnetic enhancement of nuclear relaxation occurs due to motion both of the electron spin and of the entire complex relative to the direction of the applied field. Each motion affects both the longitudinal (T_1^{-1}) and the transverse (T_2^{-1}) relaxation rates of the nuclei that are close to the paramagnetic center, although not in the same way (*19*−*23*). In the absence of significant through-bond (contact) interactions (*20*, *21*), as is the case for fluorophthalates bound to PDO, the amount of enhancement is governed by the distance-dependent dipole−dipole interaction (*19*). Thus, under favorable conditions (discussed below), a measurement of paramagnetic relaxation enhancement can yield detailed structural information.

(A) Dipolar Relaxation. Use of paramagnetic relaxation enhancement to determine metrical parameters has chiefly focused on measurement of enhancement of the longitudinal relaxation rate, T_{1M}^{-1}, of noncovalently bound ligands in rapid exchange with the bulk solution. T_{1M}^{-1} is obtained (eq 1) by correcting the observed relaxation rate (T_{1obs}^{-1}) for diamagnetic contributions (T_{1d}^{-1}).

$$T_{1M}^{-1} = T_{1obs}^{-1} - T_{1d}^{-1} \tag{1}$$

In the limit of fast exchange, the dependence of T_{1M}^{-1} on ligand concentration can be extrapolated to determine T_{1M}^{-1} for the fully bound state (*23*). However, under conditions of slow exchange, resonances for the bound state must be observed directly. This can be extremely difficult due to severe line broadening, and as a consequence, there have been few applications of paramagnetic relaxation to studies of tightly bound ligands (*12*, *24*, *25*).

Equations 2 and 3 represent the Solomon relationships that describe dipolar longitudinal and transverse relaxation, respectively (*19*, *26*). In eqs 2 and 3, μ_0 is the permittivity of free space, γ_N is the nuclear gyromagnetic ratio, g_e is the Landé *g*-factor, μ_B is the nuclear magneton, *S* is the spin quantum number of the paramagnet, and ω_S and ω_I are the electronic and nuclear angular Larmor frequencies in rads per second. Terms containing ω_S and $\omega_S \pm \omega_I$ have been collected, with the simplifying assumption that $\omega_S \gg \omega_I$.

$$T_{1M,Solomon}^{-1} = \frac{2}{15}\left(\frac{\mu_0}{4\pi}\right)^2 \frac{\gamma_N^2 g_e^2 \mu_B^2 S(S+1)}{r^6}\left(\frac{7\tau_c}{1+\omega_S^2\tau_c^2} + \frac{3\tau_c}{1+\omega_I^2\tau_c^2}\right) \tag{2}$$

$$T_{2M,Solomon}^{-1} = \frac{1}{15}\left(\frac{\mu_0}{4\pi}\right)^2 \frac{\gamma_N^2 g_e^2 \mu_B^2 S(S+1)}{r^6}\left(\frac{13\tau_c}{1+\omega_S^2\tau_c^2} + \frac{3\tau_c}{1+\omega_I^2\tau_c^2} + 4\tau_c\right) \tag{3}$$

The correlation time (τ_c) in eqs 2 and 3 is the reciprocal of a cumulative rate constant (eq 4) that includes contributions from the rates of electronic relaxation, τ_s^{-1}, molecular rotation, τ_r^{-1}, and chemical exchange of the probe nucleus, τ_M^{-1}. Inspection of eq 2 shows that an error of 1 order of magnitude in τ_c can lead to an error of up to 40% in distance. Therefore, an accurate determination of τ_c is crucial to the accuracy of the distance obtained.

$$\tau_c^{-1} = \tau_s^{-1} + \tau_r^{-1} + \tau_M^{-1} \tag{4}$$

Equation 2 is the most commonly encountered version of the Solomon relationship. The r^{-6} dependence predicted by theory has led to its widespread application for determination of the distance between a paramagnetic metal ion and a probe nucleus (*12*, *27*−*33*). The theory was derived with the basic assumptions that (1) the system has a spherically symmetric magnetic moment (i.e., an isotropic **g** tensor) and that (2) the electron spin system is in the Zeeman limit [i.e., the static zero-field splitting (zfs) energy of the complex is negligible compared to the electronic Zeeman energy]. However, in practice, it is rare that these criteria are rigorously satisfied.

Of the transition metal ions of interest in biology, those with pseudo-spherical symmetry [e.g., high-spin Mn(II)] typically have electronic correlation times (ca. 10^{-8} s) that are too slow to give detectable NMR lines. When **g** is anisotropic, the NMR probe nucleus experiences fluctuating values of both **g** and ω_S. The relaxation behavior of the probe nucleus will therefore depend on the extent to which molecular rotation averages the **g** anisotropy at a given magnetic field. Attempts have been made to include the effects of **g** anisotropy in the derivation of the relaxation equations for some axial high-spin systems (*34*, *35*). In cases where dipolar relaxation is dominant, relatively large anisotropies are expected to lead to a deviation in the overall value

of g_e^2 of only 20−30% (*36*). Thus, owing to the r^{-6} dependence of T_M^{-1}, **g** anisotropy should lead to no more than a 3−5% error in the calculated distance.

In contrast to **g** anisotropy, large zfs can lead to dramatic deviations between the observed relaxation behavior and that predicted by Solomon (*37*−*39*), particularly for integer spin systems (*39*−*43*). Sizable zero-field splittings can lead to an observed T_1 that is longer than expected and, consequently, to a distance estimate that is too large (*39*, *42*). However, in half-integer spin systems, the $m_s = \pm^1/_2$ transition, which is unaffected by zfs, will always be effective for nuclear relaxation (*37*−*39*). Consequently, at high applied field strengths ($\omega_{zfs} \leq \omega_{zeeman}$), a relatively large static zfs is expected to cause only a small perturbation (*38*). Thus, for the present studies on CoPDO at 11.7 T, deviations due to zfs are expected to be minimal.

(B) Curie Relaxation. In addition to contact and dipolar relaxation, a third relaxation mechanism is Curie relaxation (*23*). This mechanism does not involve the relaxation of the electronic spin system, although it is connected directly to the presence of unpaired electrons. The bulk susceptibility of the sample, which is related to the Boltzmann population of the electron spin levels, depends only on the average *z*-component of the spin angular momentum $\langle S_z \rangle$. Because $\langle S_z \rangle$ is already an average over the spin states, this interaction cannot be modulated by electron relaxation. Therefore, the correlation time that dominates this interaction is the rotational correlation time of the complex, τ_r (*44*, *45*).

The interaction of the nuclear spin with $\langle S_z \rangle$ is also dipolar in nature, and consequently, the energy of this interaction depends on $S(S + 1)$ and on the inverse cube of the metal−nucleus distance, while the relaxation depends on the square of these quantities. In the limit $\omega_S \tau_r \gg 1$ (a condition often met for biological macromolecules), the dipolar contributions to T_{1M}^{-1} and T_{2M}^{-1} from this mechanism are given by eqs 5 and 6, respectively.

$$T_{1M,Curie}^{-1} = \frac{2}{5}\left(\frac{\mu_0}{4\pi}\right)^2 \frac{\omega_I^2 g_e^4 \mu_B^4 S^2(S+1)^2}{(3kT)^2 r^6}\left(\frac{3\tau_r}{1+\omega_I^2 \tau_r^2}\right) \quad (5)$$

$$T_{2M,Curie}^{-1} = \frac{1}{5}\left(\frac{\mu_0}{4\pi}\right)^2 \frac{\omega_I^2 g_e^4 \mu_B^4 S^2(S+1)^2}{(3kT)^2 r^6}\left(4\tau_r + \frac{3\tau_r}{1+\omega_I^2 \tau_r^2}\right) \quad (6)$$

Comparison of eqs 2 and 5 shows that the Curie mechanism will have a negligible effect on T_{1M}^{-1} for magnetic field strengths sufficiently large that $\omega_I \tau_r \gg 1$. In contrast, the constant term of $4\tau_r$ on the right-hand side of eq 6 means that, because of the ω_I^2 term in the numerator of eq 6, the contribution of Curie relaxation to T_{2M}^{-1} will increase with the square of the applied field. Comparison of eqs 3 and 6 shows that Curie relaxation is expected to be the dominant T_2 relaxation mechanism at high field (see below).

RESULTS

ZnPDO. The 470 MHz ^{19}F NMR spectra for 3-F- and 4-F-phthalates bound to ZnPDO are shown in Figure 1. For 3-F-phthalate + ZnPDO (3F−ZnPDO), there is a sharp line at −43.6 ppm and a second broader peak at −39 ppm. The

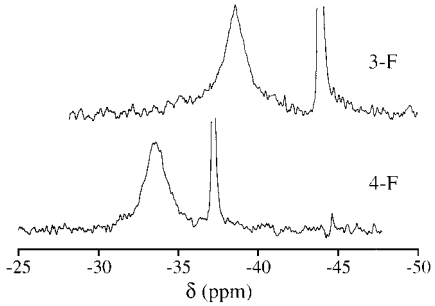

FIGURE 1: 470 MHz ^{19}F NMR spectra for fluorophthalates bound to ZnPDO. Top: 3-F-phthalate. Bottom: 4-F-phthalate.

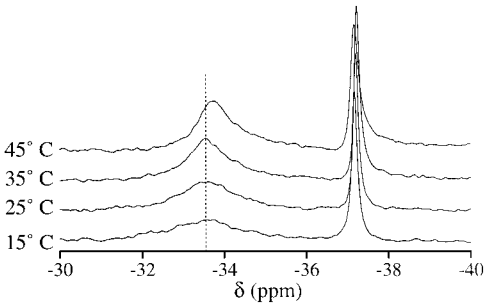

FIGURE 2: ^{19}F NMR spectra (470 MHz) recorded at various temperatures for 4-F-phthalate bound to ZnPDO. The PDO concentration was ∼2 mM; 0.9 equiv of substrate was added. Temperatures are indicated on the plot. The vertical dotted line indicates the low-temperature position of the bound peak. As the temperature is raised to 45 °C, the bound peak begins to shift toward the free 4-F-phthalate peak.

former is due to free 3-F-phthalate. The line width, $\Delta\nu_{1/2}$, of the broad −39 ppm resonance is 770 Hz, consistent with the decreased rotational rate expected for 3-F-phthalate when it is bound to the protein. On the basis of the integrated areas of the two peaks, approximately 93% of the substrate is bound under these conditions. This gives an apparent K_d of 10 μM, in good agreement with the K_d of 6.7 μM for this substrate with FePDO (*5*). A similar pattern is seen in the spectrum for 4-F-phthalate in the presence of ZnPDO (lower spectrum in Figure 1). The sharp line at −37.2 ppm arises from free 4-F-phthalate while the broad line at −34 ppm is attributed to a ZnPDO + 4-F-phthalate complex (4F−ZnPDO). The 4F−ZnPDO line width of 785 Hz is identical, within experimental uncertainty, to that for 3F−ZnPDO. Integration (see Supporting Information, Figure S4) indicates that ∼96% of the 4-F-phthalate is bound, giving a K_d of ≈1 μM, again consistent with the value of 2.2 μM for this substrate with FePDO (*5*).

The temperature dependence of the 4F−ZnPDO ^{19}F spectrum is shown in Figure 2. These data were measured in order to determine the exchange rate between bound and free substrate. The line width for the bound substrate decreases as the temperature is raised, consistent with the expected increase in the tumbling rate of the enzyme (τ_r^{-1}). From proton NMRD measurements, τ_r for PDO has been estimated to decrease from 2×10^{-7} to 9×10^{-8} s as the temperature is increased from 15 to 45 °C (*11*). This can account for the factor of 2 decrease in line width of the bound phthalate. In contrast, the width of the free phthalate resonance is ca. 20 Hz and does not change significantly below 45 °C. The chemical shift of the enzyme-bound 4-F-phthalate does not change until the temperature is raised

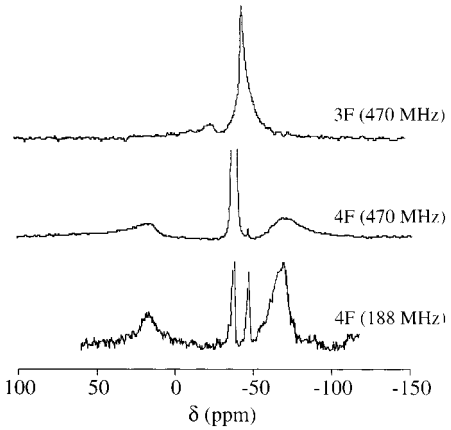

FIGURE 3: ^{19}F NMR spectra for fluorophthalates with CoPDO. Spectra were recorded at 25 °C. Top: 3-F-phthalate at 470 MHz. Center: 4-F-phthalate at 470 MHz. Bottom: 4-F-phthalate at 188 MHz.

above 35 °C. These data demonstrate that the substrate is in slow exchange below 35 °C, with the onset of detectable exchange occurring between 35 and 45 °C. An upper limit for the exchange rate, k, between two interconverting species can be estimated from the chemical shift difference ($k \ll 2\pi\Delta\nu/\sqrt{2}$; $\Delta\nu$ = line separation in hertz). At 45 °C, the peaks are separated by $\Delta\delta = 3.4$ ppm, giving an exchange rate, even at 45 °C, that is slower than 10^4 s^{-1}.

CoPDO. The 470 MHz ^{19}F NMR spectra for 3-F- and 4-F-phthalate bound to CoPDO at 25 °C are shown in Figure 3. The spectrum for 3-F-phthalate bound to CoPDO (3F−CoPDO, top spectrum in Figure 3) shows two resolvable peaks and is thus superficially similar in appearance to that of 3F−ZnPDO. The smaller peak, at −24 ppm, has a line width ($\Delta\nu_{1/2} = 5.0$ kHz) that is significantly larger than that for the diamagnetic Zn analogue. The most intense peak, with a maximum at −44 ppm, has the same chemical shift as free 3-F-phthalate. However, its line width ($\Delta\nu_{1/2} = 6.2$ kHz) is more than 300 times larger than that of free 3-F-phthalate. Satisfactory simulations of the −44 ppm peak could only be obtained by using a pair of Lorentzian functions, with line widths of approximately 6.1 and 0.2 kHz (see Supporting Information, Figure S5). The narrow component, centered at −44 ppm, is attributed to free phthalate. The 200 Hz line width is approximately 2-fold broader than that seen for other free fluorophthalate spectra, due to the rapid data acquisition and the 100 Hz apodization used in data processing.[4] The broad component (which is actually centered at approximately −47 ppm; see Supporting Information) is attributed to a paramagnetically broadened species whose chemical shift is accidentally degenerate with that of free fluorophthalate. The line width of the broad −47 ppm component is comparable to that of the −24 ppm line. This assignment is supported by inversion−recovery experiments discussed below. Therefore, two paramagnetically shifted lines are seen for 3-F-phthalate bound to CoPDO, together with the line for free 3-F-phthalate. The observation of two paramagnetically shifted lines for singly labeled 3-F-phthalate indicates that there are two distinct orientations of 3-F-phthalate with respect to the Co.

[4] The short cycle time used for measuring the spectra for CoPDO distorts the diamagnetic peaks for free fluorophthalate, preventing an estimate of K_d from NMR data.

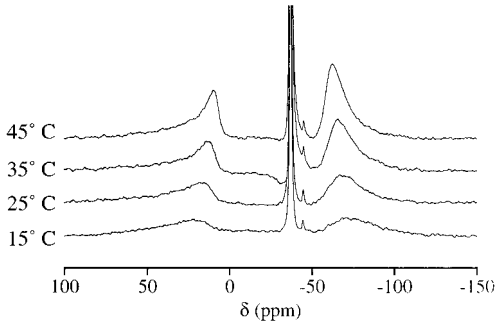

FIGURE 4: Temperature-dependent 470 MHz ^{19}F NMR spectra for 4-F-phthalate + CoPDO. Temperatures are indicated on the plot. See Figure 2 for experimental details.

The 470 MHz ^{19}F spectrum for 4-F-phthalate + CoPDO (4F−CoPDO, center spectrum in Figure 3) is more complex, with four peaks, two extremely broad lines bracketing a pair of sharp peaks. The sharp line at −37.2 ppm is attributed to 4-F-phthalate free in solution. The second sharp line at −45.0 ppm is time dependent, growing in intensity over 24−36 h. Control experiments with 4-F-phthalate in the presence of $CoCl_2$ (data not shown) give a −45.0 ppm resonance that we attribute to a weak interaction of 4-F-phthalate with the free Co(II) ion. For the CoPDO samples, the free Co(II) must arise from sample decomposition; thus, the −45.0 ppm peak provides a measure of the integrity of the samples. It was not possible to determine the relative amplitudes of the narrow and broad resonances for 4F−CoPDO due to their very different relaxation properties. However, it is clear that the −45.0 ppm peak represents a small minority of 4-F-phthalate, even after 36 h of data collection. This confirms that there is no significant sample degradation.

The two broad peaks in the 4F−CoPDO spectrum, centered at −70 and +18 ppm, have line widths of approximately 9 and 6 kHz, respectively. These are approximately an order of magnitude broader than the peak attributed to 4-F-phthalate bound to ZnPDO. This demonstrates that there is a strong magnetic interaction between 4-F-phthalate and the high-spin Co(II) ion.

The ^{19}F NMR spectrum for 4F−CoPDO measured at 188 MHz is also shown in Figure 3. At lower field, the line widths for both of the paramagnetically broadened lines decrease significantly, to 2.2 kHz. This field dependence is consistent with the expected dominance of Curie relaxation in T_2. However, the decrease is only 3−4-fold, significantly smaller than the factor of 6.25 predicted by the B_o^{-2} dependence in eq 6. Possible explanations are discussed below.

The temperature dependence of the 470 MHz NMR data for 4-F-phthalate bound to CoPDO is shown in Figure 4. These data support the conclusion that Curie relaxation dominates T_2. As the sample temperature is increased, the two broad lines associated with 4-F-phthalate bound to CoPDO sharpen and move closer together. The dipolar shifts are well described by simple Curie (T^{-1}) behavior. In addition, the dramatic decrease in line width with increasing temperature is consistent with the (T^{-1}) dependence of τ_r, the decrease in viscosity at higher T, and the factor of $(3kT)^2$ in the denominator of eq 6. Thus, the data in Figures 3 and 4 indicate that Curie spin relaxation is the dominant factor contributing to T_2, and the equations relating distance to line width should be applicable. The dominance of Curie

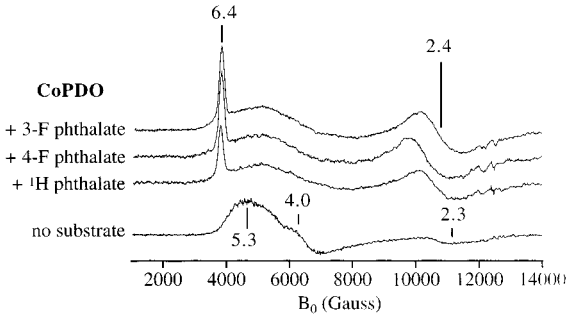

FIGURE 5: 35 GHz EPR spectra for CoPDO and for CoPDO with phthalate (^{1}H), 4-F-phthalate, and 3-F-phthalate. Spectra were collected in absorption mode under conditions of adiabatic rapid passage; numerically calculated derivatives are shown. Conditions: 2 K, 35.02 GHz, 3.2 mW microwave power, 100 kHz field modulation (2 G amplitude), 32 ms time constant, and receiver gain = 200.

relaxation is confirmed by comparison with the Solomon contribution to T_2 (see section on distance calculations).

To determine whether fluorine substitution on the phthalate affects the nature of substrate binding, EPR spectra were recorded at 35 GHz for substrate-free CoPDO and for CoPDO in the presence of phthalate, 3-F-phthalate, and 4-F-phthalate in the laboratory of Prof. Brian Hoffman (Northwestern University, Evanston, IL). The spectra (Figure 5) for CoPDO in the absence of phthalate show a highly anisotropic signal with apparent *g*-values of 2.3, 4.0, and 5.3. Addition of phthalate, 3-F-phthalate, or 4-F-phthalate results in a significant perturbation of the spectrum. For each of the phthalates, the perturbation is very similar, demonstrating that the fluorine substitution does not cause a significant perturbation of the cobalt site. The phthalate-bound spectra for CoPDO have well-defined turning points at *g*-values of 2.4 and 6.4, with a broader transition at $g \approx 5$. The spectra are consistent with a distorted high-spin Co(II) site (*46*, *47*).

Inversion Recovery Measurements. The ability to observe ^{19}F NMR signals from two different orientations for 3-F- and 4-F-phthalates bound to CoPDO made it both possible and necessary to measure independently the longitudinal relaxation rates for the pendant atoms on all four ring carbons. The 36 μs 180° pulse length restricted uniform excitation [approximately $(4t)^{-1}$] to ca. ±15 ppm from the transmitter frequency. Therefore, because of the chemical shift differences for the bound fluorophthalates (minimum separation of ~19 ppm or ~9 kHz, Figure 3), it was necessary to determine each T_1 with a separate experiment.

A summary of the T_1 measurements is given in Table 1. An example of the inversion−recovery data for 3F−CoPDO, centered at −44 ppm, is presented in part A of Figure 6. These data provide further evidence that this peak is the result of two overlapping signals and that these signals differ in T_1 by approximately 2 orders of magnitude. This is best illustrated by the spectrum at $\tau = 30$ ms (dotted line; Figure 6A). For $\tau = 30$ ms, the broad line is largely relaxed while the central narrow resonance remains inverted. Due to the overlap of these resonances, the relaxation rate of the broad component could not be determined accurately from the intensity at the peak maximum. Therefore, the T_1 value for the broad −47 ppm line was determined by monitoring the intensity at the field values marked by the vertical arrows in Figure 6A. At these fields there is minimal overlap of the two −44 ppm lines. The fits to these data are shown in the inset to Figure 6A. The fitting uncertainties are typically 1−2 ms. A more conservative estimate of the true uncertainty can be obtained by comparing the fits at different fields. All four field values show the same time dependence, with an average T_1 of 24 ms and a standard deviation in T_1 of 2 ms.

Table 1: ^{19}F NMR Results for 3-F-phthalate and 4-F-phthalate Bound to M(II)PDO (M = Co, Zn, Fe) at 25 °C[a]

metal ion	substrate	δ^b	$\delta^{hyp\,c}$	$\Delta\nu_{1/2}{}^d$	$T_1{}^e$	$T_2{}^f$	$\tau_{null}{}^g$
Zn(II)	3-F	−39		0.8		414	
	4-F	−34		0.8	1410	414	500
Co(II)	3-F	−24	+15	5.1	14	62	10
		−47	−8	6.2	24	51	15
	4-F	+18	+52	6.2	6.6	51	3
		−70	−36	8.9	4.9	36	2
	4-F[h]	+18	+52	2.2		145	
		−70	−36	2.2		145	
Fe(II)	4-F	−15	+19	15.6		20	
	3-F	−37	+2	6.3	6	51	5

[a] All data are for 470 MHz, except as indicated. [b] Observed chemical shift with respect to external trifluoroacetate (0 ppm). [c] Hyperfine shift, defined as $\delta_{obs} - \delta_{dia}$, where δ_{obs} is the observed chemical shift and δ_{dia} is the chemical shift for the diamagnetic reference. [d] FWHM, in kHz, obtained from fitting the data with a Lorentzian function (see text). [e] Longitudinal relaxation rate, in ms from fits of inversion recovery data. [f] Transverse relaxation rate, defined as $T_2 = (\pi\Delta\nu_{1/2})^{-1}$, in μs. [g] Approximate null time, in ms (see text). [h] Measured at 188 MHz.

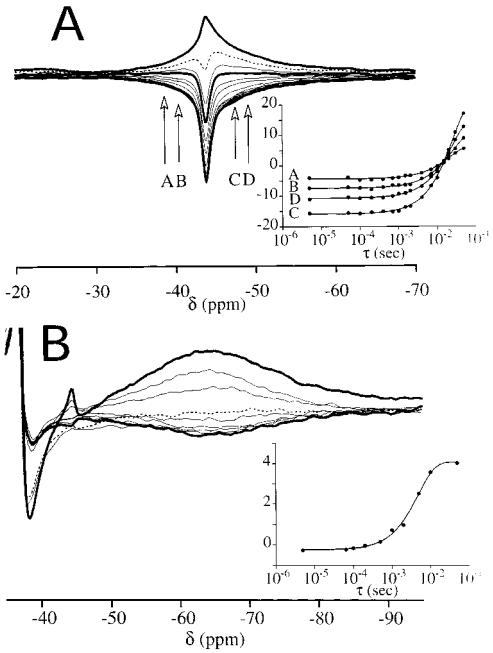

FIGURE 6: Inversion recovery data and (insets) best fits of T_1 curves to amplitude. (A) Data for the −44 ppm resonance of 3-F-phthalate + CoPDO. Spectra shown are for τ values of 5, 50, 100, 200, 400, and 700 μs and 1, 1.5, 2, 4, 7, 15, 20, 30, and 50 ms. The extreme times (5 μs and 50 ms) are shown in bold, as is the approximate null time (15 ms). The 30 ms spectrum (dashed line) shows nearly complete recovery of the broad paramagnetically relaxed peak (centered at approximately −47 ppm), while the narrow resonance corresponding to free phthalate remains inverted (see text). Vertical arrows labeled A, B, C, and D mark the fields used for T_1 calculations (inset; see text for details). (B) Inversion recovery data for the −70 ppm resonance of 4-F-phthalate + CoPDO. Spectra shown are for τ values of 5, 50, 100, 200, and 500 μs and 1, 2, 5, 10, and 50 ms. The extreme times (5 μs and 50 ms) are shown in bold. The approximate null time (2 ms) is shown dashed.

This standard deviation is a measure of the uncertainty for all of the T_1 determinations. Inversion−recovery experiments centered at −24 ppm (Supporting Information, Figure S3A) give a T_1 of 14 ms for this resonance. These values are more than 50 times shorter than the T_1 measured for ZnPDO (1.4 s, Figure S3D). This demonstrates that the diamagnetic contribution to T_1 can be no more than 2% of the total relaxation rate observed in CoPDO.

Inversion−recovery data for the −70 ppm resonance associated with 4F−CoPDO are shown in part B of Figure 6. In these measurements, the free phthalate resonance (−37.2 ppm) appears out of phase due to inhomogeneous excitation. Due to the proximity of the bound peak and the free phthalate peak ($\Delta\delta = 15$ kHz), and the inherent breadth of the bound peak (9 kHz), phase corrections were difficult. The phase corrections that were applied were chosen to minimize the baseline deviations, to both high and low frequency, within a set of spectra. The inset to Figure 6B shows the normalized intensity as a function of τ, with the best fit giving a T_1 value of 4.9 ms. The analogous experiments centered at +18 ppm (Figure S3B) did not suffer from overlap with the free phthalate resonance and gave a T_1 of 6.6 ms.

An alternative, although somewhat less accurate, estimate of T_1 can be made from the τ value that gives zero amplitude (τ_{null}). For complete inversion, $T_1 = \tau_{null}/\ln(2) = 1.44\tau_{null}$. Although the absolute value of T_1 will be different for incomplete inversion, the relative T_1 values determined from τ_{null} should be unchanged. The τ_{null} values (see Figures 6 and S3) are given in Table 1. The τ_{null} values show the same pattern that is seen for T_1. The relaxation rates for both 4-F-phthalate peaks are 3−4-fold faster than those for the 3-F-phthalate peaks, and in both phthalates, the two different orientations have relaxation rates that differ by about 50%. This is consistent with the 4-fluoro substituent being closer to the metal than the 3-fluoro substituent. It also implies that the two orientations of the substrate place the fluorine substituent at slightly different distances from the metal.

FePDO. Initial room temperature measurements on FePDO showed the presence of only one paramagnetically broadened fluorine resonance when either 3-F-phthalate (−37 ppm) or 4-F-phthalate (−17 ppm) was bound, in contrast with the two paramagnetically broadened lines seen for CoPDO. To explore the origin of this difference, NMR spectra were measured as a function of temperature for 3F−FePDO and 4F−FePDO. For 3-F-phthalate bound to FePDO (Figure 7A), the broad −37 ppm resonance sharpens and shifts to lower field as the temperature is raised. On the basis of the temperature dependence of its chemical shift, it can be concluded that the −37 ppm resonance may be in exchange with an unobserved resonance at very low field. At temperatures above 35 °C, a weak, unresolved peak is seen at approximately −38 ppm. The origin of this peak is unclear. It is unlikely that this peak is due to the other orientation of bound 3-F-phthalate, however, since its chemical shift and line width appear to be temperature independent. In addition, the line width of the −38 ppm peak (ca. 1.1 kHz from Lorentzian fits) is substantially smaller than that of the principal, −37 ppm resonance and substantially smaller than the line widths of the corresponding 3F−CoPDO resonances. The T_1 of the −37 ppm resonance for 3F−FePDO at 25 °C (Figure S3C) is 6 ms.

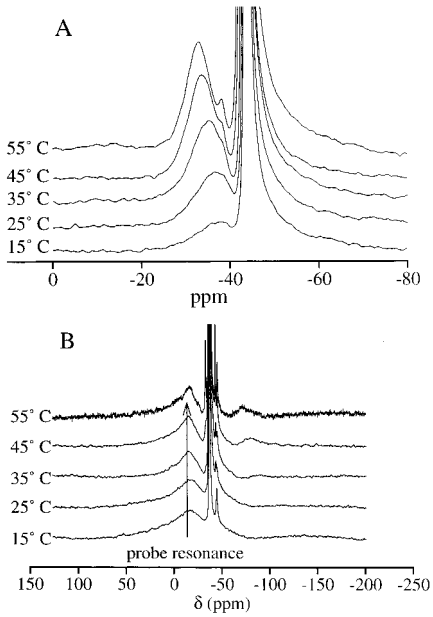

FIGURE 7: ^{19}F NMR spectra (470 MHz) recorded at various temperatures for fluorophthalates bound to FePDO. Temperatures are as indicated. (A) 3-F-phthalate. (B) 4-F-phthalate. The vertical arrow in part B indicates the position of the probe resonance (see text).

The spectra for 4-F-phthalate bound to FePDO (4F−FePDO) have a broad, asymmetric peak at approximately −15 ppm, together with two narrow lines at approximately −40 and −48 ppm (Figure 7B). The narrow lines are attributed to free phthalate and phthalate interacting with unbound Fe(II), in analogy with the assignments of the narrow lines for CoPDO. The broad line at −15 ppm presumably represents the paramagnetically broadened resonance from either one or both of the fluorines. However, interpretation of this line is complicated by the presence of the probe resonance at −15 ppm. Close examination of the probe response for a sample lacking fluorophthalate (Figure S1) shows that, as expected, the probe resonance is temperature independent. In contrast, the broad −15 ppm resonance for 4F−FePDO sharpens considerably and moves slightly upfield as the temperature is increased. This demonstrates that the peak at −15 ppm is, in fact, a superposition of the probe resonance with a broad peak attributable to 4-F-phthalate bound to FePDO, with the 4-F-phthalate resonance only becoming readily detectable at higher temperatures. The presence of the probe resonance precluded measurement of relaxation data for this sample.

In addition to the low-field feature, a second broad peak becomes detectable at higher field (∼−70 ppm) at temperatures above 35 °C. The high-field peak sharpens and shifts downfield as the temperature is raised further. The fwhm of this peak at 45 °C (9.0 kHz) is identical to the apparent line width (corrected for the probe contribution) of the low-field resonance at this temperature. We attribute these two peaks to two different orientations of 4-F-phthalate bound to FePDO. The observation of two broad peaks with dipolar shifts of opposite sign is reminiscent of the behavior observed when either 3-F-phthalate or 4-F-phthalate is bound to CoPDO.

Distance Calculations. Solving the Solomon equation (eq 2) for the metal−nucleus distance, r, gives eq 7 for

longitudinal relaxation. Similar treatment of the Curie equation (eq 6) for transverse relaxation gives eq 8.

$$T_1: \quad r = \left(\frac{2}{15}\left(\frac{\mu_0}{4\pi}\right)\gamma^2 g_e^2 \mu_B^2 S(S+1)(T_{1M})\left(\frac{7\tau_c}{1+\omega_s^2\tau_c^2} + \frac{3\tau_c}{1+\omega_I^2\tau_c^2}\right)\right)^{1/6} \quad (7)$$

T_2:

$$r = \left(\frac{1}{5}\left(\frac{\mu_0}{4\pi}\right)\frac{\omega_I^2 g_e^4 \mu_B^2 S^2(S+1)^2}{(3kT)^2}\left(4\tau_r + \frac{3\tau_r}{1+\omega_I^2\tau_r^2}\right)T_{2M}\right)^{1/6} \quad (8)$$

In the absence of significant exchange contributions, both the Solomon equation for T_1 and the Curie relation for T_2 should provide reliable distance information.

Inserting the values of the constants in eq 7 gives

$$r = (1.074 \times 10^{-43}(T_{1M})(f(\tau_c)))^{1/6} \quad (9)$$

In eq 9, $f(\tau_c)$ represents the rightmost term in parentheses in eq 7. While the value of $f(\tau_c)$ can, in principle, be determined experimentally by measuring the relaxation enhancement as a function of magnetic field, a field-dependent determination would have been prohibitive for these samples due to the difficulty of observing the protein-bound ^{19}F resonances at the lower field values. However, given that τ_s for high-spin Co(II) is expected to be between 1 and 10 ps (*23, 48*) and assuming that τ_s dominates τ_c (see eq 3), the value of $f(\tau_c)$ is expected to be between 4.3×10^{-12} ($\tau_c = 1$ps) and 3.0×10^{-11} ($\tau_c = 10$ ps). These give apparent Co−F distances, R_{M-F}, of 4.7 Å ($\tau_c = 1$ ps) to 6.5 Å ($\tau_c = 10$ ps) for the fluorine that gives rise to the −47 ppm resonance in 3F−CoPDO. The corresponding R_{M-F} values for the −24 ppm resonance in 3F−CoPDO are 4.3−6.0 Å. The analogous calculations for 4-F-phthalate bound to CoPDO give 3.6−5.0 Å (−70 ppm resonance) and 3.8−5.3 Å (+14 ppm resonance). The uncertainty in R_{M-F} due to the 10−20% uncertainty in T_1 is significantly smaller than the uncertainty due to $f(\tau_c)$. Although the uncertainty in $f(\tau_c)$ introduces uncertainty into the distance calculations, the *relative* distances are directly comparable. Any errors in $f(\tau_c)$ should cancel for relative distance comparisons, since $f(\tau_c)$ is expected to be the same for all four resonances. Thus the ratio of, for example, the longest to the shortest distances, $R_{Co-3F,-44}/R_{Co-4F,-64} = 1.31$, is considerably more precise than either distance alone.

The τ_s values estimated here allow us also to calculate the contribution of Solomon relaxation to T_2 (eq 3) and to compare it with that for Curie relaxation. From this, we estimate that Solomon relaxation contributes less than 1% of the total T_2 relaxation, thereby confirming that Curie relaxation is dominant. Therefore, an estimate of the individual distances for the two orientations for 4-F-phthalate bound to CoPDO can also be obtained from the T_2 data using eq 8. The τ_r values reported previously (*48*) (0.20, 0.14, 0.11, and 0.09 μs at 15, 25, 35, and 45 °C, respectively) give Co−4F distances of 4.0, 4.4, 4.7, and 4.7 Å for the downfield signal and 4.0, 4.1, 4.2, and 4.3 Å for the upfield signal. The apparent temperature dependence of these distances is, of course, nonphysical. We attribute this to the presence of another exchange process that increases the line widths, and thus decreases the apparent distances, at lower temperatures. This could involve, for example, different suborientations within the substrate-binding pocket. Such a process is expected to be independent of magnetic field and would appear as a constant offset to the field-dependent line width. An exchange rate of 10^3 s^{-1} would be sufficient to explain the smaller than expected reduction in line width for 4F−CoPDO on going from 470 to 188 MHz.

Table 2: Temperature-Dependent ^{19}F NMR Results for Fluorophthalates Bound to Co(II)PDO, Fe(II)PDO, and Zn(II)PDO Measured at 470 MHz

	T (°C)	δ^a	$\Delta\nu_{1/2}{}^b$	$T_{2M}{}^c$	$R_{M-F}{}^d$	δ^a	$\Delta\nu_{1/2}{}^b$	$T_{2M}{}^c$	$R_{M-F}{}^d$
4F−Co	15	23	14.0	25.4	4.0	−73	15.1	23.4	4.0
	25	18	6.2	63.6	4.4	−70	8.9	41.4	4.1
	35	13	3.2	138	4.7	−67	5.7	66.2	4.2
	45	10	2.6	167	4.4	−63	3.6	110	4.7
3F−Fe	15	−37	3.9	133	6.2				
	25	−37	3.6	133	5.8				
	35	−35	3.2	138	5.5				
	45	−34	2.7	159	5.4				
	55	−33	2.6	122*	5.2				
4F−Fe	15	−16							
	25	−17	15.6	22.1	4.3				
	35	−15	9.2	38.3	4.4				
	45	−15	9.0	40.3	4.3	−80	9.0	40.3	4.3
	55	−14	6.6	48.2*		−72	4.9	65.0*	
Zn−4F	15	−30	1.2						
	25	−30	0.8						
	35	−30	0.7						
	45	−30	0.6						

[a] Chemical shifts relative to external trifluoroacetate (0 ppm). [b] Full width at half-maximum, in kHz, from fits of a Lorentzian line shape to the data. [c] $T_{2M} = (T_{2obs}^{-1} - T_{2d}^{-1})^{-1}$ in μs. The values given for ZnPDO + 4-F-phthalate are taken as T_{2d}. Values marked with an asterisk (*) are not corrected for diamagnetic contributions. [d] R_{M-F}, in Å, calculated from the equation for Curie T_2 relaxation (eq 8), using the rotational correlation times given in ref. (*11*).

Within the assumptions of eq 8, the T_2 derived distances are likely to be more accurate than those obtained from T_1, since even a 50% error in the estimated line width will give a distance error of less that 0.5 Å. It is thus reassuring that the T_2 derived distances are well within range of 3.6−5.3 Å estimated from the T_1 data. Although they may be more accurate, the T_2 derived distances are likely to give *less* accurate estimates of the ratio of distances. This is because background subtraction errors, which are the limiting feature of the T_2 derived distances, will not generally cancel for comparisons of two peaks, while τ_c errors, which limit the T_1 derived distances, will cancel. Nevertheless, the T_1 and T_2 derived distance ratios are also in good agreement (1.05 vs 1.09 for the two different R_{M-4F} values).

Unfortunately, reliable T_2 data could not be obtained for Co−3F due to the overlap of the free 3-F-phthalate resonance with the upfield resonance of bound 3-F-phthalate. However, T_2 data could be used to estimate the Fe−F distances in FePDO (Table 2). The Fe−3F data for one orientation give apparent distances of 6.2, 5.8, 5.5, 5.4, and 5.2 Å at temperatures of 15−55 °C. The higher temperature values are in good agreement with the 4.3−6.5 Å range calculated from the T_1 data for CoPDO. The ratio of the 45 °C distances for 4F−FePDO (4.3 Å) and 3F−FePDO (5.4 Å) is also in good agreement with the ratio of R_{Co-3F} to R_{Co-4F} obtained

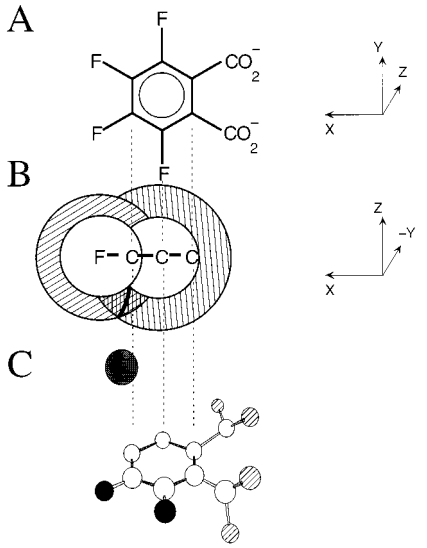

FIGURE 8: Geometric model showing the placement and orientation of the phthalate ring with respect to the mononuclear metal ion. (A) View in the *xy* plane. The coordinate system employed places the origin at the center of the phthalate ring, with the *y*-axis passing through the 3-F. (B) View in the *xz* plane. The intersection between the *xz* plane and spheres that restrict the position of the metal ion relative to the 3-F and the 4-F are shown as crosshatched areas. (C) Molecular view of the model (CS Chem3D Pro) with the Fe(II) 4.5 Å from the 4-F and 5.5 Å from the 3-F. The Fe is shown in gray, the 3-F and 4-F are in black, and the carboxylate oxygens are in crosshatch. Vertical dashed lines mark the *x* coordinates of the phthalate ring carbons.

from the T_1 data (1.26 for the T_2 data vs 1.22 for the average distances found in the T_1 measurements).

A Geometric Model for CoPDO + Phthalate Based on the T_1 Measurements. Each of the NMR-derived M−F distances defines a sphere centered on one of the fluorine atoms. In principle, it would be possible to use the distance constraints to define a volume within which the metal lies. Such a construction is, however, difficult to visualize and, moreover, difficult to justify, given the uncertainties in the measurements. Consequently, we have taken a more intuitive, qualitative, approach. The first observation is that all of the fluorines show strong relaxation, resulting in similar R_{Co-F} values. This immediately indicates that the metal must be displaced from the phthalate plane. If the metal were in the phthalate plane, R_{Co-3F} and R_{Co-4F} would differ significantly, resulting in more dramatically different relaxation rates. Because the two different R_{Co-3F} distances and the two different R_{Co-4F} distances are nearly the same, the metal must be approximately on the plane perpendicular to and bisecting the phthalate ring. We have used this as a starting point to construct an approximate model of the phthalate−metal interaction.

A coordinate system was defined with the center of the phthalate ring at the origin, the phthalate ring lying in the *xy* plane and the *y*-axis passing through the 3- and 6-carbons (Figure 8A). On the basis of the known dimensions of the fluorophthalate ring (*49*) (2.73 Å from the center of the ring to the fluorine), this coordinate system places the 3-F at (0, ±2.73, 0) and the 4-F at (2.36, ±1.39, 0). The M−3F distance constrains the metal ion to lie between two spheres of radius 4.3 and 6.5 Å (using the extremes for the two different 3-F positions), centered on 3-F. The intersection of these two spheres with the *xz* plane defines a ring given by eq 10.

$$3.3^2 \leq x^2 + z^2 \leq 5.9^2 \tag{10}$$

The T_1 measurements for 4-F further constrain the metal ion to lie between spheres of radius 3.3 and 5.1 Å, centered on the 4-F (2.36, 1.39, 0). The intersection of these spheres with the *xz* plane defines a second ring, given by eq 11.

$$3.3^2 \leq (x - 2.36)^2 + z^2 \leq 5.1^2 \tag{11}$$

These two rings are shown in Figure 8B. The metal must lie within the intersection of these rings (crosshatched area in Figure 8B). If the additional constraint that $R_{M-3F}/R_{M-4F} \approx 1.2$ is added, the cobalt should lie on the arc connecting the extreme points (bold line in Figure 8B).

If we now relax the bilateral symmetry constraint, it is apparent that a displacement of the cobalt toward one of the 3-F positions by approximately 0.2 Å would be sufficient to explain the observed asymmetry in T_1 and T_2. Figure 8C shows a molecular model of the Fe(II) and the phthalate with the 4-F being 4.5 Å and the 3-F being 5.5 Å from the Fe(II).

DISCUSSION

Comparison of CoPDO and FePDO. The CoPDO samples are the most spectroscopically accessible. Therefore, it is important that the Co(II) enzyme−substrate complex is representative of the catalytically competent Fe complex. Several points suggest that this is indeed the case. The binding constants for Co(II) and Fe(II) to PDO are very similar, the binding constants for phthalate, 3-F-phthalate, and 4-F-phthalate to FePDO and CoPDO are similar, and the enhancements of phthalate binding in the presence of metal or of metal binding in the presence of phthalate are similar for Fe(II) and Co(II) and all three phthalates (*5*). The 4-F-phthalate + FePDO data show a pair of signals with shifts of opposite sign, similar to those seen for 4F−CoPDO. The dipolar shifts and line widths are both larger with FePDO than they are with CoPDO, consistent with the larger spin on iron.

For 3-F-phthalate + FePDO, a second resonance is not clearly resolved even at 55 °C. The T_1 of 6.3 ms for the −37 ppm resonance of 3F−FePDO is slightly shorter than the corresponding T_1 values for CoPDO, consistent with the larger spin and shorter T_{1e} of Fe(II). Using 6.3 ms and $S = 2$ for high-spin Fe(II) in eq 7 gives an estimate of 4.3−6.8 Å for the Fe to 3-F distance for τ_c values between 0.3×10^{-12} and 3.0×10^{-12}. This range is in reasonable agreement with that determined for CoPDO, given the uncertainty in the correlation times.

Interpretation of Handedness in Substrate Binding. Because the fluorophthalates used in these studies are labeled in only one position, binding of the asymmetric monofluorophthalates to PDO is expected to show handedness (i.e., with the fluorine label facing "left" or "right"), and the two orientations need not be either magnetically or thermodynamically equivalent. This is confirmed for both 3-F-phthalate and 4-F-phthalate bound to CoPDO. In contrast, only a single peak is observed for fluorophthalates bound to ZnPDO. Although only one of the two possible orientations

might be occupied for ZnPDO, this would be inconsistent with the observation of similar K_d values for phthalate binding to Zn- and CoPDO (*5*).

A more likely explanation is that the two phthalate orientations are not resolvable for the diamagnetic ZnPDO complex. The maximum chemical shift difference between the two unresolved lines can be no more than the observed line width. This is 800 Hz (1.7 ppm) for ZnPDO. An alternative estimate of the maximum chemical shift difference for fluorophthalate bound to ZnPDO can be obtained by assuming that the chemical exchange rate is approximately the same as that found for the Co derivatives (ca. 10^3 s^{-1}). Two different signals will be averaged if they differ by less than 1 ppm. In either case, the maximum difference in the chemical shift between the two putative conformations would be 1−2 ppm. The observed chemical shifts for ^{19}F span several hundred parts per million, with changes in solvent polarity causing changes in chemical shift of as much as 12 ppm (*50*). Thus, the fact that two distinct orientations are not resolved for ZnPDO implies that the substrate-binding pocket has sufficiently uniform polarity that, for the zinc complex, the two different phthalate orientations have chemical shifts that differ by less than 1−2 ppm. The much larger chemical shift differences for the different CoPDO orientations are attributable to dipolar shifts induced by the paramagnetic Co(II).

The magnitude of the dipolar shift depends both on R_{M-F} and on the orientation of the M−F vector with respect to the metal ion **g**-tensor (*51*). Given the approximate symmetry of R_{M-F}, differences in distance are not sufficient to account for the difference in dipolar shifts for a given fluorophthalate. It is likely, instead, that the pattern of chemical shifts reflects differences in the orientation of the different M−F vectors relative to the Co(II) **g** tensor. The asymmetry in the observed paramagnetic shifts for 3F−CoPDO ($\Delta\nu/\nu_0 = +15, -8$ ppm) and 4F−CoPDO ($\Delta\nu/\nu_0 = +52, -36$ ppm) indicates that the orientation of the Co−3F and Co−4F vectors, and therefore the plane of the phthalate ring, must be rotated relative to the **g**-tensor axes in CoPDO.

Differentiation of Binding Orientations. The two different orientations are not equally populated. Integration of the Lorentzian fits of the 470 MHz 4F−CoPDO data indicates that the −70 ppm resonance is approximately twice (2.1 ± 0.2) as intense as its analogue at +18 ppm. The 188 MHz data, which did not suffer from the baseline roll associated with the 470 MHz data, also indicate a ratio of 2:1. For 3F−CoPDO, the ratio of the high-field (−47 ppm) to low-field (−24 ppm) areas is significantly greater (5.5 ± 0.3). Electrostatic repulsion, for example between a negatively charged protein site and the fluorine substituent, may contribute to the asymmetry in binding. However, this is unlikely to be the major source of the asymmetry, given apparently uniform binding site environments (i.e., identical chemical shift values) that are seen for ZnPDO. Rather, we suggest that this asymmetry reflects differences in steric interactions, with one of the 3-F positions being slightly more crowded. Energetic differences of 4 kJ/mol (3-F) and 1.7 kJ/mol (4-F) would be sufficient to explain the observed population differences. The observation of less asymmetry for 4-F-phthalate is consistent with the fact that the increase in K_d for 4-F-phthalate relative to phthalate is smaller than the increase for 3-F-phthalate. The observation of less hindrance at the 4-fluoro site suggests a more open binding pocket at this site, consistent with the need for oxygen and its reactive intermediates to bind in a region close to the 4-C. The ability to observe different binding orientations, together with the availability of a variety of substituted substrate analogues (*5*), provides further opportunities to characterize the substrate-binding pocket and will be the subject of future studies.

Mechanistic Implications of the Three-Dimensional Model. PDO has been the subject of a number of mechanistic (*5*) and biophysical (*7*−*11*) studies, and the necessity of the nonheme ferrous ion for catalysis in this family of dioxygenases has been known for some time (*52*). Previous studies of substrate binding to PDO have examined the effects of phthalate binding on the spectroscopic properties of the mononuclear metal ion (*8*−*10*). These studies showed a decrease in the coordination number of the mononuclear metal ion on binding of phthalate and further suggested that this occurs without coordination of the phthalate to the Fe. The present NMR studies directly probe the interaction between phthalate and the mononuclear metal ion by observing the effect of the metal ion on the spectroscopic properties of the substrate.

The geometric model generated from the relaxation data is fully consistent with the likely mechanism of hydroxylation (*14*). The model in Figure 8 that is derived from these spectroscopic measurements places the metal ion almost directly above the 4- and 5-carbons of the substrate. The next step in catalysis is believed to be the binding of oxygen. Even at the lowest distance limit, there is sufficient room to accommodate O_2 binding to the metal in either an end-on or a side-on fashion. The reaction catalyzed by PDO results in the addition of *cis*-hydroxyls to both the 4- and 5-carbons of phthalate. Thus, a model that places the metal ion directly over the bond that is attacked can readily explain the observed stereochemistry.

ACKNOWLEDGMENT

We thank Dr. Kimber Clark-Baldwin for extensive measurements that provided the genesis of this project. In addition, we thank Prof. Brian Hoffman for the use of his instruments, Dr. Shifi Kababya for her assistance in obtaining the Co EPR spectra, Dr. Bruce Palfey for synthesis of 4-fluorophthalate, and Prof. Robert R. Sharp for many helpful discussions regarding data analysis.

SUPPORTING INFORMATION AVAILABLE

A detailed description of the background subtraction (Figures S1 and S2), the inversion recovery data not shown in the main paper (Figure S3), area determination for free and bound 4-F phthalate + ZnPDO (Figure S4), and Lorentzian peak resolution for the −44 ppm peak for 3F−CoPDO (Figure S5). This material is available free of charge via the Internet at http://pubs.acs.org.

REFERENCES

1. Hagedorn, S. R., Hanson, R. S., and Kunz, D. A., Eds. (1988) *Microbial Metabolism and the Carbon Cycle*, Harwood Academic Press, New York.
2. Batie, C. J., LaHaie, E., and Ballou, D. P. (1987) *J. Biol. Chem. 262*, 1510−1518.

3. Bull, C., and Ballou, D. P. (1981) *J. Biol. Chem. 256*, 12673−12680.
4. Ballou, D. P., and Batie, C. J. (1988) in *Oxidases and Related Redox Systems* (King, T. E., Mason, H. S., and Morrison, M., Eds.) pp 211−226, Alan R. Liss, Inc., New York.
5. Gassner, G. T. (1995) Ph.D. Thesis, University of Michigan.
6. Batie, C. J., and Ballou, D. P. (1990) *Methods Enzymol. 188*, 61−70.
7. Coulter, E. D., Moon, N., Batie, C. J., Dunham, W. R., and Ballou, D. P. (1999) *Biochemistry 38*, 11062−11072.
8. Tsang, H. T., Batie, C. J., Ballou, D. P., and Penner-Hahn, J. E. (1996) *J. Biol. Inorg. Chem. 1*, 24−33.
9. Gassner, G. T., Ballou, D. P., Landrum, G. A., and Whittaker, J. W. (1993) *Biochemistry 32*, 4820−4825.
10. Pavel, E. G., Martins, L. J., Ellis, W. R., and Solomon, E. I. (1994) *Chem. Biol. 1*, 173−183.
11. Bertini, I., Luchinat, C., Mincione, G., Parigi, G., Gassner, G. T., and Ballou, D. P. (1996) *J. Biol. Inorg. Chem. 1*, 468−475.
12. Crull, G. B., Kennington, J. W., Garber, A. R., Ellis, P. D., and Dawson, J. H. (1989) *J. Biol. Chem. 264*, 2649−2655.
13. Kauppi, B., Lee, K., Carredano, E., Parales, R. E., Gibson, D. T., Eklund, H., and Ramaswamy, S. (1998) *Structure 6*, 571−586.
14. Que, L., Jr., and Ho, R. Y. N. (1996) *Chem. Rev. 96*, 2607−2624.
15. Neidle, E. L., Hartnett, C., Ornston, L. N., Bairoch, A., Rekik, M., and Harayama, S. (1991) *J. Bacteriol. 173*, 5385−5395.
16. Jiang, H., Parales, R. E., Lynch, N. A., and Gibson, D. T. (1996) *J. Bacteriol. 178*, 3133−3139.
17. Werst, M. M., Davoust, C. E., and Hoffman, B. M. (1991) *J. Am. Chem. Soc. 113*, 1533−1538.
18. Mailer, C., and Taylor, C. P. S. (1973) *Biochim. Biophys. Acta 322*, 195−203.
19. Solomon, I. (1955) *Phys. Rev. 99*, 559−565.
20. Bloembergen, N. (1957) *J. Chem. Phys. 27*, 572−573.
21. Bloembergen, N. (1957) *J. Chem. Phys. 27*, 595−596.
22. Bloembergen, N., and Morgan, L. O. (1961) *J. Chem. Phys. 34*, 842−850.
23. Banci, L., Bertini, I., and Luchinat, C. (1991) *Nuclear and Electron Relaxation*, VCH, Weinheim.
24. Williams, T. J., and Falk, M. C. (1986) *J. Biol. Chem. 261*, 15949−15954.
25. Steinebach, V., De Jong, G. A., Wijmenga, S. S., De Vries, S., and Duine, J. A. (1996) *Eur. J. Biochem. 238*, 683−689.
26. Abragam, A. (1961) *The Principles of Nuclear Magnetism*, Oxford University Press, Oxford.
27. Jacobs, R. E., Singh, J., and Vickery, L. E. (1987) *Biochemistry 26*, 4541−4545.
28. Griffin, B. W., and Peterson, J. A. (1975) *J. Biol. Chem. 250*, 6445−6551.
29. Mildvan, A. S. (1977) *Acc. Chem. Res. 10*, 246−252.
30. Mildvan, A. S., and Gupta, R. K. (1978) *Methods Enzymol, 49*, 322−359.
31. Mildvan, A. S., Granot, J., Smith, G. M., and Liebman, M. N. (1980) *Adv. Inorg. Biochem. 2*, 211−236.
32. Crull, G. B., and Goff, H. M. (1993) *J. Inorg. Biochem. 15*, 181−192.
33. Bertini, I., and Luchinat, C. (1986) *NMR of Paramagnetic Molecules in Biological Systems*, Benjamin/Cummings Publishing, Menlo Park, CA.
34. Sternlicht, H. (1965) *J. Chem. Phys. 42*, 2250.
35. Dwek, R. A. (1973) *Nuclear Magnetic Resonance in Biochemistry*, Clarendon Press, Oxford.
36. Bertini, I., Briganti, F., Luchinat, C., Mancini, M., and Spina, G. (1985) *J. Magn. Reson. 63*, 41−55.
37. Bertini, I., Luchinat, C., Mancini, M., and Spina, G. (1984) *J. Magn. Reson. 59*, 213−222.
38. Bertini, I., Luchinat, C., Mancini, M., and Spina, G. (1985) in *Magneto-Structural Correlations in Exchange Coupled Systems* (Gatteschi, D., Kahn, O., and Willett, R. D., Eds.) Reidel, Dordrecht.
39. Bertini, I., Galas, O., Luchinat, C., and Parigi, G. (1995) *J. Magn. Reson. A 113*, 151−158.
40. Lindner, U. (1965) *Ann. Phys. 16*, 319−330.
41. Sharp, R. R. (1990) *J. Chem. Phys. 93*, 6921−6928.
42. Bayburt, T., and Sharp, R. R. (1990) *J. Chem. Phys. 92*, 5892−5899.
43. Bertini, I., Capozzi, F., Luchinat, C., Nicastro, G., and Xia, Z. (1993) *J. Phys. Chem. 101*, 198−201.
44. Vega, A. J., and Fiat, D. (1976) *Mol. Phys. 31*, 347.
45. Gueron, M. (1975) *J. Magn. Reson. 19*, 58−66.
46. Bencini, A., Bertini, I., Canti, G., Gatteschi, D., and Luchinat, C. (1981) *J. Inorg. Biochem. 14*, 81−93.
47. Abragam, A., and Pryce, M. H. L. (1951) *Proc. R. Soc. London 206*, 173−191.
48. Bertini, I., Luchinat, C., and Messori, L. (1987) in *Metal Ions in Biological Systems* (Sigel, H., Ed.) pp 47−86, Marcel Dekker, Inc., New York.
49. Gowda, D. S. S., and Rudman, R. (1983) *Acta Crystallogr. C 39*, 582−584.
50. Emsley, J. W., and Phillips, L. (1971) in *Progress in NMR Spectroscopy* (Emsley, J. W., Phillips, L., and Sutcliffe, L. H., Eds.) Pergammon Press, New York.
51. Kurland, R. J., and McGarvey, B. R. (1970) *J. Magn. Reson. 2*, 286−301.
52. Yamaguchi, M., and Fujisawa, H. (1980) *J. Biol. Chem. 255*, 5058.

BI990431Y